Supporting Information

Gianoli et al. 10.1073/pnas.1713135114

Effect of the Single-Channel Gating Swing

In the classical gating-spring model, the single-channel gating swing is necessary for channel gating; it is indeed the relaxation of the tension in the tip link that favors the open state of the channel. In the model presented here, however, channel gating is controlled also by the differences in energy between the membrane conformations corresponding to the three states of the channel pair, which favor the OO configuration at small interchannel distances (Fig. 2*D*). In Fig. 3, we have demonstrated that without the elastic membrane potentials, the channels do not open. In Fig. S1, we investigate the role of the single-channel gating swing δ in the presence of the potentials by plotting open probability vs. displacement curves while varying the value of this parameter. We can see that the displacement range over which the channels gate increases as δ decreases (orange to black curves). This result stems from the fact that, at fixed imposed displacements, the gain in elastic energy from channel opening is greater for larger values of δ. However, and most importantly, even with a vanishing value of this parameter, the channels do gate, and the open-probability curve remains roughly sigmoidal (black curve). This result demonstrates that, contrary to the classical model, the single-channel gating swing is not required in our model. When $\delta = 0$, channel gating is uniquely triggered by the differences in elastic energy of the lipid bilayer deformations, which depend on the channels' conformations and favor the OO state at small interchannel distances (Fig. 2*D*).

Slow Adaptation and the Parameter X_0

Myosin motors in stereocilia regulate tip-link tension in a process called slow adaptation, presumably by dragging the tip link's insertion point along the side of the taller stereocilium (49, 50). In our model, the amount of tension exerted by the tip links is set by the parameter X_0, since the force exerted by the tip link on its two branches reads $f_t = k_t[\gamma(X - X_0) - d - l]$ (main text). This parameter therefore takes a constant value for each curve mimicking fast measurements for which the myosin motors do not have the time to adapt, but can be varied between different curves to simulate the effect of slow adaptation over longer time scales. In Fig. S2, we generate force–displacement curves for different values of X_0, starting from a given default value $\bar{X}_0$. As X_0 varies, the force–displacement curve shifts diagonally while preserving its shape. This result is in agreement with experimental measurements in spontaneously oscillating hair bundles, where force–displacement curves were measured after slow adaptation had the time to take place (8, 59).

Change of Force–Displacement Relation After Fast Adaptation, and Effect of Ca^{2+} Concentration

By keeping X_0 constant, but changing the value of the channel gating energy E_g, it is possible to simulate the behavior of a cell for which only fast adaptation takes place. The force–displacement curves in Fig. S3 compare the mechanics of a hair bundle before and after the onset of fast adaptation. Channel adaptation is modeled as an increase in the gating energy by 1 $k_B T$ between the blue and the light-blue curves, as we did to generate the twitch curves in Fig. 5 (34, 35). We can see that the range of displacements associated with negative stiffness narrows as the gating energy increases. For a variation of E_g of 1 $k_B T$ though (blue and light-blue curves), the two ranges are similar, but the value of the force changes for the same imposed displacement, as experimentally observed (59). Increasing further the value of the gating energy eventually suppresses the region of negative stiffness (yellow curve). Such a force–displacement relation has been measured in high Ca^{2+} concentration (10).

Effect of the Length of the Tip-Link Fork on the Open Probability and the Twitch

We investigate here the effect of an increased length of the tip-link fork as observed at the upper end of the tip link (19). With longer branches, for the same interchannel distance, the angle between the two branches is smaller. We therefore expect channel motion within the membrane plane to produce only relatively small changes in tip-link extension. In Fig. S4, we show the curves of the open probability vs. displacement and the twitch amplitude vs. external force with a length of the tip-link fork $l = 80$ nm. This value is in agreement with electron micrographs of the tip link's upper end (19). We use both the default value of the interchannel distance at rest ($a_{adapt} = 26$ nm), as well as a larger value ($a_{adapt} = 80$ nm) to allow for a greater fork angle. For the default value and in the presence of the membrane elastic potentials (orange curve), the curve is roughly sigmoidal, but the channels gate over a range of displacements that is 10 times larger than what is typically measured. When a_{adapt} is increased to 80 nm (black curve), the gating range is even larger. Finally, in the absence of the elastic membrane potentials (red curve), the channels remain closed, similar to what is observed in Fig. 3. The twitch amplitudes are dramatically reduced compared with the typical values obtained in Fig. 5 and peak at much larger forces.

Effect of the Adaptation Springs' Stiffness and the Membrane Potentials' Amplitude on the Open Probability and the Twitch

We present in Fig. S5 a study of the sensitivity of our results to the variation of some specific parameters. Some parametric variations have already been studied in Figs. S1, S3, and S4, where we show, respectively, the dependence of the open probability on the single-channel gating swing δ, the dependence of the force–displacement relation on the channel gating energy E_g, and the effects of the parameters l and a_{adapt} on the open probability and on the twitch amplitude as a function of force. In Fig. S5, we focus on the influence of the value of the adaptation springs' stiffness and the membrane potentials' amplitude, which directly affect the relative movement of the coupled MET channels in our model. More specifically, we investigate the influence of these two parameters on the probabilities of the different states of the channel pair (OO, OC, and CC) and on the global open probability as functions of hair-bundle displacement, as well as their influence on the twitch amplitude as a function of the external force applied to the hair bundle. Three values of the adaptation-spring stiffness are chosen ($k_a = 0.5$, 1 and 5 mN·m^{-1}), which include our default value of 1 mN·m^{-1}. To vary the magnitude of the elastic membrane potentials, we define a global scaling factor that is common to the three potentials OO, OC, and CC, and which reaches 100% for the default parameters given in Table 1 and corresponding to the plots of Fig. 2*D*. Five different amplitudes of the membrane potentials are investigated, as specified by the values of this scaling factor above each column of the figure.

When the adaptation-spring stiffness is sufficiently high ($k_a =$ 5 mN·m^{-1}; Fig. S5, *Top*), the channels are maintained far from each other by the adaptation springs in a region where the elastic membrane potentials are nearly flat and therefore play a

negligible role. In this case, the channels gate independently, as shown from the substantial values of the probability of the OC configuration for intermediate hair-bundle displacements. Consequently, the range of displacements over which the channels gate—some 600 nm—is much larger than observed experimentally, where it is ∼100 nm (44–47). Furthermore, the amplitude of the twitch is very small, <1 nm.

When the adaptation-spring stiffness corresponds to our chosen default value ($k_a = 1$ mN·m^{-1}; Fig. S5, *Middle*), the membrane potentials are necessary to open the channels. The range over which the channels gate narrows and the amplitude of the twitch increases with increasing values of the scaling ratio. For a scaling ratio of 100%, we recover the curves shown in Figs. 3 and 5, for the default set of parameters (orange box). The superimposition of the P_{open} and P_{OO} curves as well as the flat P_{OC} curve indicate that channel gating is cooperative.

Finally, when the adaptation-spring stiffness is sufficiently low ($k_a = 0.5$ mN·m^{-1}; Fig. S5, *Bottom*), the relative influence of the membrane potentials is dominant, and the overall shape of the probability curves changes rapidly with the scaling ratio.

In summary, these results show that very different behaviors can be generated in our model by varying a small number of parameters. It is possible, however, to identify a range of realistic parameters supported by the literature, for which the different observables simultaneously match the experimentally measured ones.

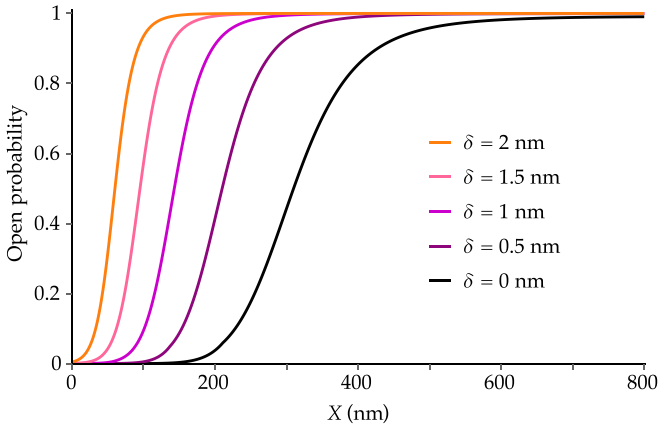

Fig. S1. Open probability–displacement relations for different values of the single-channel gating swing δ. The orange, reference curve corresponds to the orange curve of Fig. 3, where $\delta = 2$ nm. The other curves are obtained by varying δ, while keeping the remaining parameters fixed. The corresponding values of δ are indicated directly in the figure.

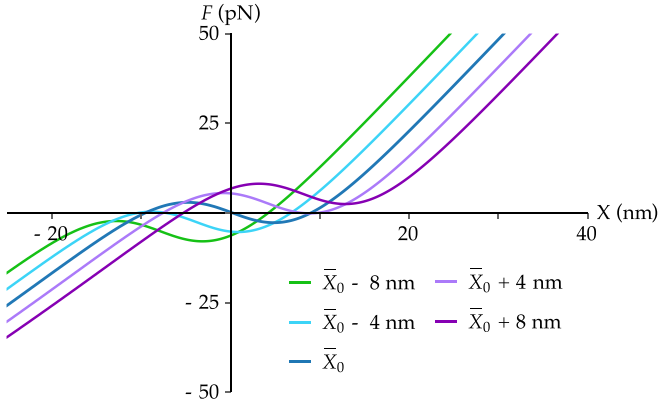

Fig. S2. Force–displacement relations for different values of X_0. The blue curve associated with the default value $X_0 = \bar{X}_0$ is obtained by using the same set of parameters as the blue curve in Fig. 4*A*. The other curves are obtained with the same set of parameters, except for the values of X_0, which are indicated directly in the figure.

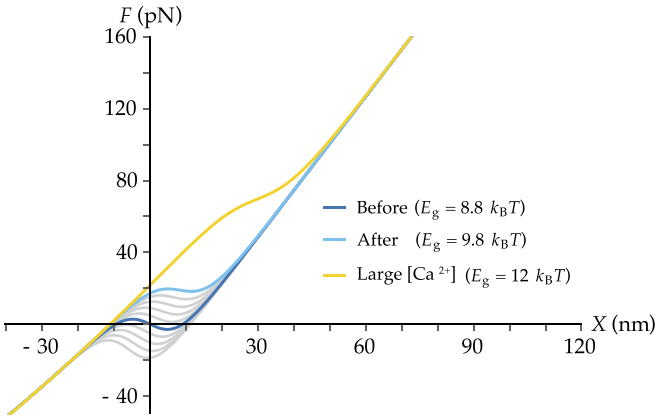

Fig. S3. Force–displacement relations for a hair bundle presenting a region of negative stiffness, with different values of the channel gating energy E_g. The blue curve ($E_g = 8.8\ k_BT$) is obtained by using the same set of parameters as the blue curve in Fig. 4*A*. The other curves are obtained by changing the value of E_g. Two other particular curves are highlighted: The light blue curve ($E_g = 9.8\ k_BT$), characterized by an increase in E_g by 1 k_BT, mimics a force–displacement relation measured immediately after most channels have closed in a cell for which only fast adaptation is at play. The yellow curve ($E_g = 12\ k_BT$) mimics the effect of a high calcium concentration.

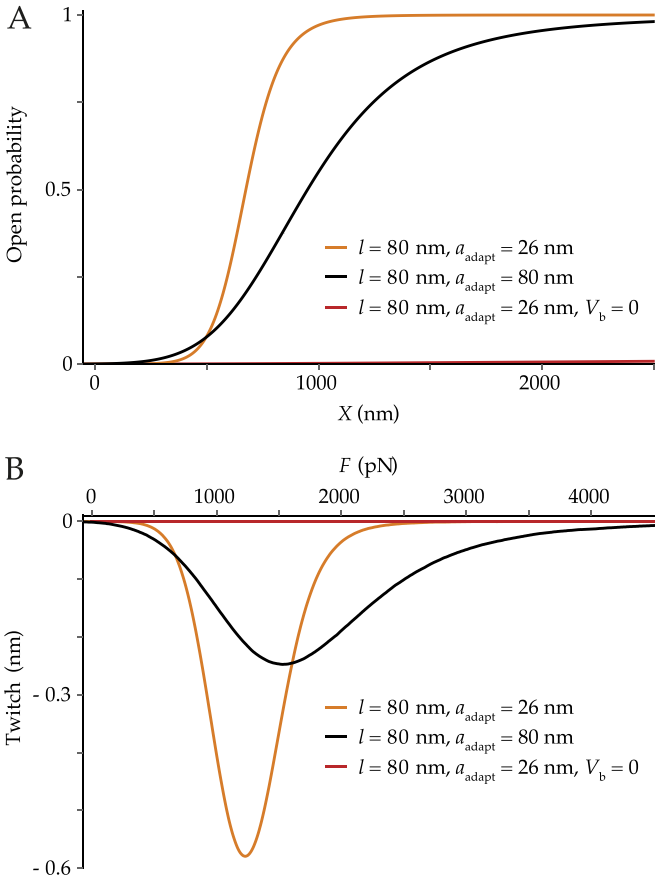

Fig. S4. Channel open probability as a function of hair-bundle displacement (*A*) and twitch amplitude as a function of the external force (*B*) for a long tip-link fork. The orange curves here have been generated by using the same set of parameters as the one used to generate the default, orange curve of Fig. 3, except for the parameter *l*, which has been set to 80 nm. The other parameters that change between the three sets of curves are indicated directly in the figure.

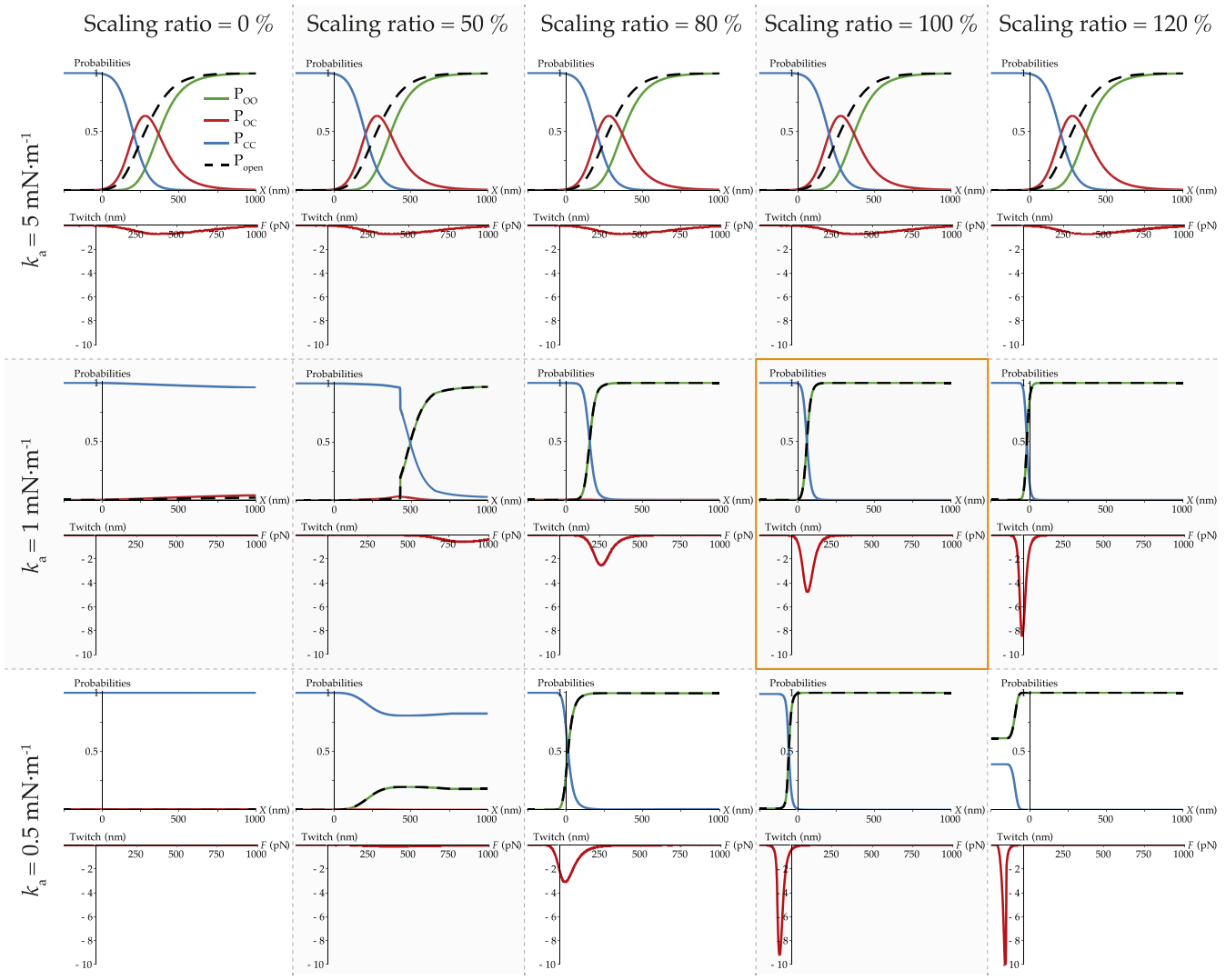

Fig. S5. Parametric-variation study for different values of the adaption-spring stiffness and amplitudes of the elastic membrane potentials. In the upper part of each of the 15 chosen parameter sets, we represent the probabilities P_{OO}, P_{OC}, and P_{CC} of the three states of the channel pair (OO, OC, and CC), as well as the global open probability P_{open}, as functions of the hair-bundle displacement X. The amplitude of the twitch as a function of the external force F exerted on the hair bundle is shown below each upper image. Three different values of the adaption-spring stiffness k_a are chosen, as indicated on the left of each row. Five amplitudes of the membrane potentials are investigated, characterized by a scaling factor as indicated on the top of each column. This scaling factor is equal to the common ratio of the amplitudes E_{OO}, E_{OC}, and E_{CC} used here to those used as default parameters in Table 1 and shown in Fig. 2*D*. The color and line styles for the different probabilities are indicated directly in the top-left panel.

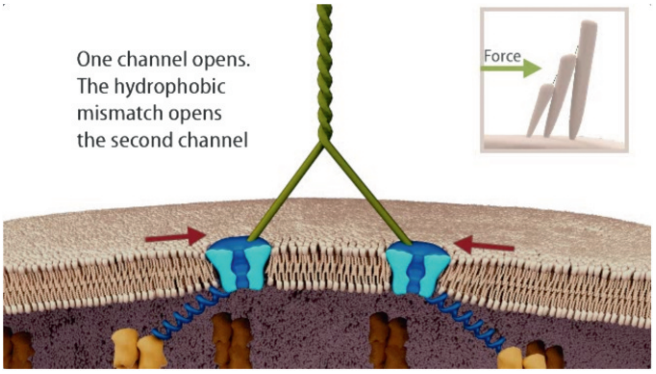

Movie S1. Dynamic illustration of cooperative gating mediated by the lipid bilayer in a two-channel mechanotransduction model. Animation realization: IlluScientia.

Movie S1